Machine-learning-based size estimation of marine particles in holograms recorded by a submersible digital holographic camera.

LIU, Z., GIERING, S., THEVAR, T., BURNS, N., OCKWELL, M. and WATSON, J.

2023

Machine-Learning-based Size Estimation of Marine Particles in Holograms Recorded by a Submersible Digital Holographic Camera

Zonghua Liu[1,*], Sarah Giering[1,**], Thangavel Thevar[2], Nick Burns[3], Mike Ockwell[3], and John Watson[2]

[1] National Oceanography Centre, Southampton, UK
[2] School of Engineering, University of Aberdeen, Aberdeen, UK
[3] Hi-Z 3D LTD, London, UK

***Abstract*—Particle size estimation is key to understanding carbon fluxes and storage in the marine ecosystem. Images of particles provide much information about their size. A subsea digital holographic camera was used to image particles in vertical trajectory in South Georgia. The holograms were processed using a rapid hologram processing suite that extracted focused particle vignettes from these raw holograms. A machine-learning-based method has been developed to analyse the particle size information from these vignettes. To be specific, a structured-forest-based model trained on a group of synthetic holographic particle images is used to detect the particle edges in these vignettes. Following that, a set of pixel-wise morphology operators are used to extract particle regions (masks) from their edge images. Lastly, the size information of the recorded particles can be calculated based on these mask images. The proposed method has been evaluated on a group of synthetic holograms and real holograms, compared with the other ten methods, including four edge-based methods, four region-based methods, a thresholding-based method, and a Kmeans-based method. The results show that our method has the best performance regarding accuracy and processing time. It reaches ∼0.7 of mean IoU and ∼25 s of running time on the 1,000 test vignettes. In terms of qualitative analysis, the regions of the given examples extracted by the proposed method closely match the real particle regions. We also use this method to analyse the size distributions of two profiles, and some generic results are given in this paper.**

***Index Terms*—subsea digital holography, size estimation, particle size distributions, hologram processing, machine learning**

I. Introduction

Accurate determination of the size and abundance of particles in the ocean, such as plankton and detritus, is critical for understanding the ocean food web and carbon cycle. A critical parameter when analysing ocean plankton and particles is size, as size strongly influences the role of organisms in the marine food web [1] and the role of particles in ocean carbon storage [1-3]. Recent advances in technology now allow broad-scale monitoring of plankton and particles in situ using underwater camera systems [4-6]. Images of particles provide much information about their abundance and size. However, while the collection of images has advanced rapidly, the analysis of these images is still relatively slow, leading to often long delays (up to years) between image collection and interpretation. In addition, correctly determining the size of an imaged particle remains a challenge [7].

Lensless in-line digital holography (LIDH) [8] is an advanced technique which has been widely used to image microscale marine particles [9] (typically micrometre to millimetre scale) due to its high resolution (typically several micrometres), large depth-of-field (several millilitres in LIDH [10]), and large sampling volume (typically in the scale of millilitres). While other imaging techniques, such as photography, usually rely on high-magnification lenses to image small particles in good resolution, which causes a significant reduction of the depth-of-field and by reference, the sampling volume. Large depth-of-field imaging can resolve the issue of particle size bias introduced by measuring particles at a limited depth-of-field (where the particles are potentially out of focus) [8,11].

Accurate particle region extraction from holograms is key to estimating the size of particles imaged by a holographic camera. Traditional image processing methods (e.g. thresholding [7]) typically struggle to segment particle regions from holographic images due to increased background noise. Machine learning has been shown to be an efficient approach for image segmentation in images with a noisy background [12-14]. However, this approach requires many human annotations for training which is generally time-expensive: to generate accurate training data, humans typically have to carefully trace objects of interest to ensure that all target pixels are included. With good training data typically requiring hundreds of images or even more, such workflows can be impractical for holograms owing to time-consuming reconstruction and auto-focusing. An alternative to human-generated training data is synthetic holographic data created based on the masks of existing particle images. Such a method reduces the time not only for reconstructing and auto-focusing particles in holograms because their recording distances are known but also for the annotations of particle regions. Here, we explore whether synthetic holograms are a useful alternative to human-annotated training data for image segmentation and object

* zonghua.liu@noc.ac.uk
** s.giering@noc.ac.uk

region extraction in holograms.

In inline holography, the silhouette of a particle is mainly recorded, that is, the edge information of a particle is more reliable than its inner information in the image [15]. In addition, substantial noise is distributed across the entire image, and this could result in worse segmentation when more pixels are involved. Therefore, it should be more reliable to segment holographic images based on particle edges than regions. Owing to high accuracy, good generalisation, fast speed and no requirement on the input size, the state-of-the-art edge detection method based on a structured forest [16] is used to detect the particle edges in reconstructed holograms, which is trained on a group of synthetic holographic data. The particles' regions (masks) are then extracted from their edge images, and their size is calculated based on the extracted masks. Three main contributions are made in this paper:
(1) Produce a synthetic holographic training dataset of marine particles and explore whether it is an alternative to human-annotated training data for object edge detection in hologram.
(2) Investigate eleven region extraction methods, and compare their performance on synthetic and real holograms.
(3) Develop a pipeline for extracting the size information of marine particles from holograms recorded by a holographic camera regarding accuracy and time efficiency.

This set of approaches have been used to analyse the PSDs of two vertical profiles imaged in an open ocean site.

II. Data Collection and Processing

A commercial submersible digital holographic camera (LISST-HOLO, Sequoia, US; some of its optical and configuration parameters [17] are given in TABLE I) was deployed to collect vertical profiles of marine particles near South Georgia (cruise DY086) as part of the UK COMICS (Controls over Ocean Mesopelagic Interior Carbon Storage [18]) programme in Nov/Dec 2017. This camera records high-resolution inline holograms of microscale particles using a collimated laser beam. The camera was mounted on the "Red Camera Frame" and deployed to 230 m in each profile recording a hologram with a volume of 1.86 mL every 1.2 - 2.5 m. Two profiles (Event 034 with 695 holograms and Event 098 with 253 holograms) from this cruise are used to evaluate the performance of the proposed size estimation method.

TABLE I
Some optical and configuration parameters of LISST-HOLO. The camera records inline holograms using the collimated beam from a 658 nm laser. The recording distance range from the sensor is 28 - 78 mm in the air. The sensor (hologram) dimension is 1600 × 1200 pixels, and its pixel pitch size is 4.4 μm.

Parameters	Values
wavelength	658 nm
illuminating light	collimated beam
recording structure	inline
Recording distance range from the sensor (in the air)	28 - 78 mm
hologram dimension	1600 × 1200
pixel pitch size	4.4 um
particle size range	25 - 2500 um

To visualise the recorded particles in digital holograms, the holograms need to be first reconstructed numerically on a computer using a reconstruction algorithm, such as Angular Spectrum [8]. Additionally, a focus measure [19] is needed to detect focussed images of recorded particles.

The particle image extraction suite (named FastScan) [20] developed by the University of Aberdeen, can rapidly reconstruct and auto-focus inline holograms recorded using collimated laser beams, and output the vignettes of imaged particles. FastScan uses Angular Spectrum as the reconstruction algorithm. It also has a robust algorithm based on contour gradient [15] to auto-focus and extract recorded particles in holograms. The algorithms are implemented using parallel computation on a powerful Field Programmable Gate Array (FPGA) such that it demonstrates a very high processing speed (838 Mp/s [20]).

FastScan was used to process the holograms of the two profiles in this work. 3257 and 1572 particle vignettes were extracted from the holograms in Events 034 and 098 respectively, and several extracted particles are shown in Fig. 1.

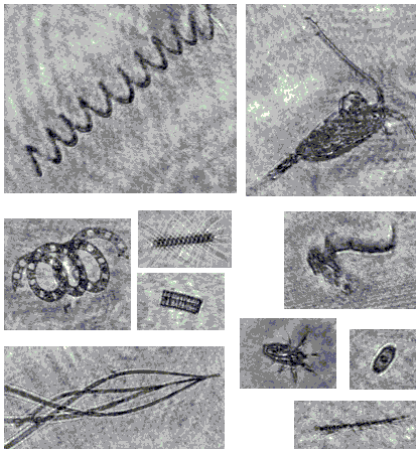

Fig. 1. Sample particle vignettes extracted by FastScan in the two profiles showing different types of plankton and particles. Note the intricate details on a noisy background.

III. Methodology

In our work, the workflow consists of three steps for estimating particles' size in their vignettes, as shown in Fig. 2. First, a set of synthetic holographic data is created as the training data, including reconstructed particle vignettes and their ground-truth edge images. Secondly, the edge-detection model is trained using the training dataset. Lastly, the trained model is used to detect particles' edges in real holograms, and a morphology operation is then carried out on the edge images to estimate the size information of the particles.

A. Synthetic holographic data

Each synthetic hologram is simulated based on the parameters of LISST-HOLO (TABLE I). Marine particle images recorded by ZooScan [21] are adopted as the target images to simulate holograms due to their noiseless background and

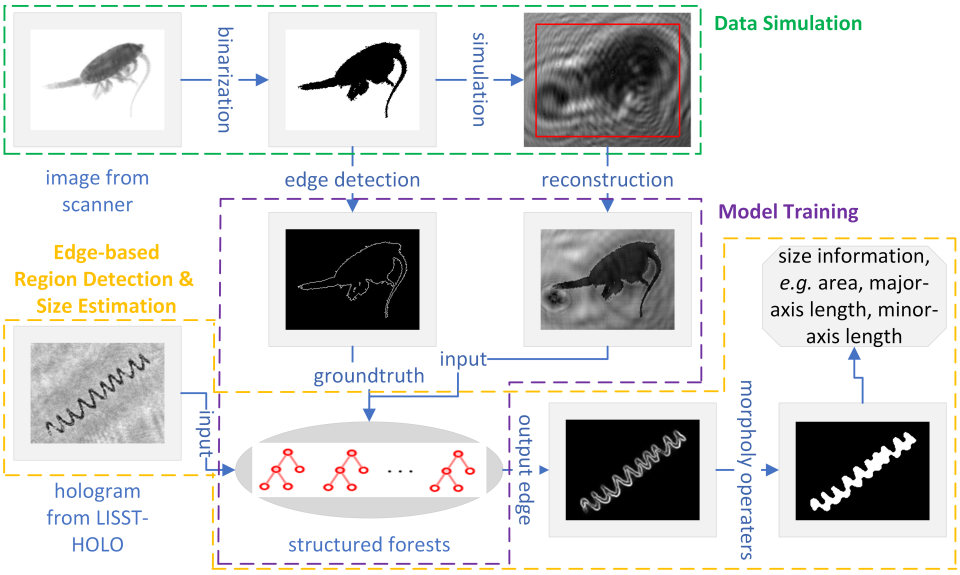

Fig. 2. Workflow to estimate the size information of particles in the particle vignettes. Three steps are contained in this workflow: data simulation in the green box, model training in the purple box, and edge-based region detection and size estimation in the orange box.

similar shape and resolution to objects imaged by LISST-HOLO. 877 marine particles imaged by ZooScan are binarised and used as the target pool. To simulate a synthetic hologram, up to 10 particles are randomly selected from the pool and their recording distances are randomly decided within the system's recording optical path (28 and 78 mm depth from the camera sensor in the air). Each particle is positioned at least 50 pixels away from each edge of the hologram. Details of each particle in its synthetic hologram (size, location and recording distance from the sensor) are stored. The dimension of each full-size synthetic hologram is the same as the holograms recorded by LISST-HOLO (1600 $\times$ 1200 pixels). Holograms are simulated using the Angular Spectrum method. Noise is added to the simulated holograms by taking real holograms without any targets and superimposing them as background noise in the simulated holograms.

B. Edge detection

The authors in [16] built a random forest consisting of eight decision trees. In each tree, the maximum depth is 64, and the numbers of positive and negative patches are 5x105. To increase the diversity of the trees and edge-detection accuracy, the trees are trained independently and the features and splits are randomly subsampled when training each node in each tree. Structured learning was used to map the edges between the input and output images in each tree. The eight trees are combined as a random forest to achieve robust outputs, and the overlapping edge maps are averaged to obtain a soft edge response. Piotr and Lawrence shared their codes on https://github.com/pdollar/edges.

C. Region extraction and particle size estimation

The edge-detection model outputs the soft edges for each input particle image, that is, in the output edge image, a pixel with a higher value could be an edge pixel with a higher probability, as shown in Fig. 3. Therefore, the output edge images from the model need to be further processed before extracting the particle size information from them.

A set of pixel-wise morphology operators are used on the outputted edge images. Since each edge image has high contrast between the particle edges and the background (Fig. 3), Otsu [22], a very fast binarisation method based on the intra-class variance between the foreground and background is used to determine the edge pixels in each edge image. To obtain the particle mask, the operation of hole filling is used to fill the holes surrounded by edges in the binarised edge image. Subsequently, two steps are implemented to remove regions that are too small: image opening using a disk-shaped structure element with a diameter of 5 pixels [1] and removing the regions that are smaller than 25 pixels [1]. The last step is to merge the regions which are within 5 pixels distance from each other in the binary image. The particle regions/masks are then extracted from the original edge image. The particle size features in a given vignette can now be calculated based on the extracted regions.

In this work, the equivalent spherical diameter (ESD) [7] is adopted to describe the size of particles. This concept describes the size of an irregularly shaped object using the diameter of a sphere which has the same area as the object. It is calculated as:

$$\mathrm{ESD} = \sqrt{A_p/\pi} \tag{1}$$

where A_p is the area of the particle which is calculated as $A_p = \sum_{i,j} R(i,j) \times (4.4\ \mu m)^2$ with R indicating a particle

[1] $25\ \mu m/4.4\ \mu m \approx 5$ and $\pi(25\ \mu m/2)^2/(4.4\ \mu m)^2 \approx 25$, where 25 μm is the minimum recognition size and 4.4 μm is the pixel pitch size in LISST-HOLO.

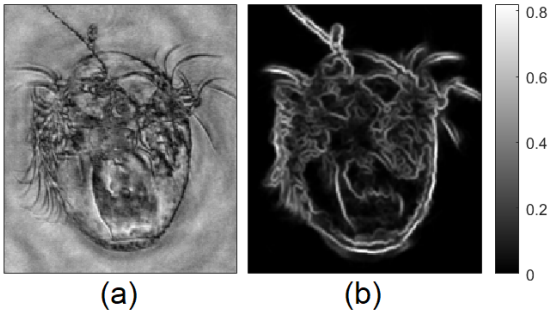

Fig. 3. A plankton hologram (a) and its soft edges (b) detected by the model. The sidebar in (b) indicates the intensity of each pixel's response as an edge pixel: a pixel with a higher value could be an edge pixel with a higher probability.

mask image and 4.4 μm indicating the pixel pitch size of LISST-HOLO. Since LISST-HOLO can only detect particles whose ESDs are in the range from 25 to 2500 μm, those particles whose ESDs are not in this range are omitted when estimating particle size.

IV. Edge Detection and Region Extraction

A. Image datasets

Two datasets are used to evaluate the performance of the edge detection model. Since the structured forest trained on the Berkeley Segmentation Data Set 500 (abbreviated to BSDS500) [23] shows good generalisation [16], this dataset is used in our work to check if the model trained on it could enable edge detection in holograms. The other one is comprised of synthetic holographic images.

BSDS500. This dataset is a standard benchmark for edge detection. It consists of 500 natural images with annotated boundaries collected from 30 human subjects. Amongst them, 200 images are used for training, 100 for validation, and the remaining 200 for testing. Since the purpose is to detect particle edges in holograms in this work, 500 images are all used as the training data.

Synthetic holographic data (SHD). One thousand synthetic holograms are created using the method described in Section III-A. Each simulated hologram is reconstructed at the distances where the particles are recorded. Each particle's holographic vignette is extracted from its reconstructed hologram based on its target image size and location in the raw hologram. 3,000 particles are randomly selected as the other training dataset. We choose this number because the performance of trained models on edge detection doesn't obviously change when more than 3,000 particles are used to train the model in our test. Their reconstructed holographic vignettes and edge images are used as the input and ground-truth images when training the model, as shown in Fig. 2.

1,000 pairs of reconstructed particle vignettes and edge images are randomly selected from the synthetic dataset as the testing data. They are used to test the edge detection performance of the structured forest. Their mask images are also needed when testing the region extraction performance of the proposed method.

Real holographic data. The 3257 and 1572 particle vignettes are respectively extracted from the holograms in the profiles of 034 and 098. Their size is calculated using the proposed method.

B. Evaluation measures

As well as time efficiency, the accuracy efficiency of region extraction is evaluated using the Intersection over Union (IoU). IoU is a primary metric to measure the accuracy of region extraction, and it is computed as the ratio of the overlap of the predicted region (r) and ground truth (gt) to their combination, as:

$$\mathrm{IoU}(r, gt) = \mathrm{TP}/(\mathrm{TP} + \mathrm{FP} + \mathrm{FN}) \tag{2}$$

where TP indicates the intersected area between r and gt as $\mathrm{TP} = r \cap gt$, FP indicates the predicted area r out of gt as $\mathrm{FP} = r \cup gt - gt$, and FN indicates the area in gt but not in r as $\mathrm{FN} = r \cup gt - r$. A perfect overlap of predicted region r and ground truth region gt has an IoU of value 1.

Since the structured forest outputs the soft edges (not binary edge image) of inputs, IoU cannot describe the accuracy of edge detection. Therefore, the Structural Similarity Index Measure (SSIM) [24] is used to evaluate the performance of edge detection. SSIM measures the similarity between two images based on three features: luminance, contrast, and structure. Therefore, it can better evaluate the image similarity than measures that are calculated only based on the intensity of corresponding pixels in two images. SSIM=1 indicates that the two images are the same; the smaller the value is, the more different the two images are. SSIM is calculated as

$$\mathrm{SSIM}(r, gt) = \frac{(2\mu_r\mu_{gt} + C_1)(2\sigma_{r,gt} + C_2)}{(\mu_r^2 + \mu_{gt}^2 + C_1)(\sigma_r^2 + \sigma_{gt}^2 + C_2)} \tag{3}$$

where μ and σ indicate the mean value and standard deviation of an image, $\sigma_{r,gt}$ is the covariance of two images; C_1 and C_2 are two small constants to stabilise the division with a weak denominator that are calculated by $C_1 = (K_1 L)^2$ and $C_2 = (K_2 L)^2$ where $K_1 = 0.01$, $K_2 = 0.03$, and $L = 255$ for 8 bits/pixel images.

All the algorithms used in this work are interpreted using MATLAB R2022a (license: 40924637), and they run on a computer with a processor of 11th-Gen Intel(R) Core(TM) i7-11850H and RAM of 32 GB.

C. Test and results

Effect of training data on edge detection: Since the structured forest shows a good generalisation in the original work, we want to check if the model trained on the dataset of BSDS500 could also work well on detecting particle edges in holographic data. Four training datasets are prepared: BSDS500 (the standard benchmark dataset of 500 images), SHD500 (a subset of 500 images randomly selected from the training synthetic holographic dataset), SHD3000 (the

whole training synthetic holographic dataset of 3,000 images) and BSDS500+SHD3000 (a combination of BSDS500 and SHD3000). The model is trained on each training dataset, and the trained models are then tested on the test dataset of 1,000 synthetic particle holograms. The output edge images are compared with the corresponding ground-truth images using SSIM. The performance results are shown in TABLE II. The model trained on SHD500 outperforms the model trained on BSDS500, which shows that it is necessary to train the model on holographic data when it is used to detect particle edges in holographic images. In theory, training the model with more data would result in better performance. No improvement is apparent when more than 3,000 images are used. The models trained on SHD3000 and (BSDS500+SHD3000) give nearly the same mean similarity value. Therefore, it is unnecessary to train the model with extra non-holographic data. In the following work, the model trained on SHD3000 will be used.

TABLE II
PERFORMANCE EVALUATION OF THE MODEL ON EDGE DETECTION ON THE TEST SYNTHETIC DATASET WHEN IT IS TRAINED ON THE FOUR DIFFERENT DATASETS.

Training datasets	BSDS500	SHD500	SHD3000	BSDS500+ SHD3000
Mean SSIM in test data	0.7028	0.8257	0.8319	0.8322

It is worth mentioning that on each training dataset, five models are trained, and they give the same SSIM value when running on the synthetic test data. This result shows that the structured forest is easy to be trained, and the trained models perform consistently well.

Comparison with other methods on region extraction: In the proposed method, the structured forest model (trained on SHD3000) is used to detect object edges and the pixel-wise morphology operation (described in Section III-C) is carried out to extract regions from given images. The proposed method is compared with ten other methods in terms of region extraction on the test dataset (1,000 vignettes), including four edge-based methods (cannyEdge, sobelEdge, prewittEdge, robertsEdge; [25] in each method, the corresponding edge detector(s) are used to detect object edges, and the proposed morphology operation is used to extract the regions based on their edges), four region-based methods (activeContour [26], and regionGrowing [27], SRegionMerging [28], watershed [29]), a thresholding-based method (OtsuThresholding [30]), and a Kmeans-based method (KMeans) [31]. The two steps described in Section III-C are lastly used to remove too small regions in outputted masks from each compared method.

TABLE III shows the region extraction performance of all the methods on the test dataset in terms of accuracy and running time. The mean of IoU measures accuracy, and the standard deviation (std) reflects robustness in this work. The proposed structured-forest-based method for region extraction significantly outperforms the other 4 edge-based methods in terms of accuracy and robustness. SRegionMerging is the best region-based method, and its mean IoU of 0.6798 is slightly smaller than structuredForest's value of 0.6922. But, its robustness is lower compared with structuredForest (0.2721 and 0.1491, respectively). Similarly with KMeans, though the mean of IoU (0.6661) is close to structuredForest, its std of IoU (0.2596) is larger than structuredForest. Amongst the 4 methods whose mean of IoU is higher than 0.6 (structuredForest, SRegionMerging, KMeans, OtsuThresholding), OtsuThresholding performs the worst with a mean of IoU of 0.6205. Regarding the running time, except for activeContour and SRegionMerging (473.1 seconds and 396.4 seconds, respectively), the remaining 9 methods can all process 1,000 particle images within 50 seconds. Although structuredForest is not the fastest method whose running time is $\sim$11.55 seconds, it is still acceptable costing $\sim$25 seconds to process 1,000 images even in the real-time data processing. Overall, the proposed method performs the best amongst the given methods in extracting regions from images in the test dataset.

TABLE III
PERFORMANCE OF THE METHODS ON REGION EXTRACTION ON THE TEST SYNTHETIC DATASET (1,000 IMAGES) IN TERMS OF THE EFFICIENCY OF ACCURACY AND TIME. THE HIGHLIGHTED VALUES INDICATE THE BEST RESULT BASED ON THE CORRESPONDING MEASURE.

Methods	**mean of IoU**	**std of IoU**	**Running time** * **(s)**
structuredForest	0.6922	0.1491	25.28
cannyEdge	0.4692	0.2672	13.28
sobelEdge	0.5301	0.3555	11.55
prewittEdge	0.5363	0.3525	11.76
robertsEdge	0.4692	0.2672	13.37
activeContour	0.4136	0.3196	473.1
regionGrowing	0.2368	0.2488	396.4
SRegionMerging	0.6798	0.2721	41.09
waterShed	0.5942	0.3132	25.02
OtsuThresholding	0.6205	0.2980	14.68
KMeans	0.6661	0.2596	19.62

* The average image size in the test dataset is 127 $\times$ 387.

Since it is difficult and time-consuming to prepare a group of benchmark regions in real particle holograms, quantitative evaluation of the eleven methods mentioned above on region extraction is not implemented in the real holographic dataset. We randomly selected five images and ran the methods on them. Their resultant regions are shown in Fig. 4. Qualitatively analysed, the performance rank of the methods is similar to the results when they ran on the test synthetic dataset: regionGrowing (in (h)) performs the worst; cannyEdge (in (c)), robertsEdge (in (f)), and activeContour (in (g)) fail to exact the particle regions except for in the last image; structuredForest (in (b)), SRegionMerging (in (i)), OtsuThresholding (in (k)), and KMeans (in (l)) outperform the other methods to extract the regions from the five examples; amongst them, structuredForest appears to be the best method, and the extracted regions most closely match the particle areas in the original images, even when there is more than one particle in the image.

Based on all the results shown in this section, the proposed method has the capability to rapidly extract the particle regions from holographic images.

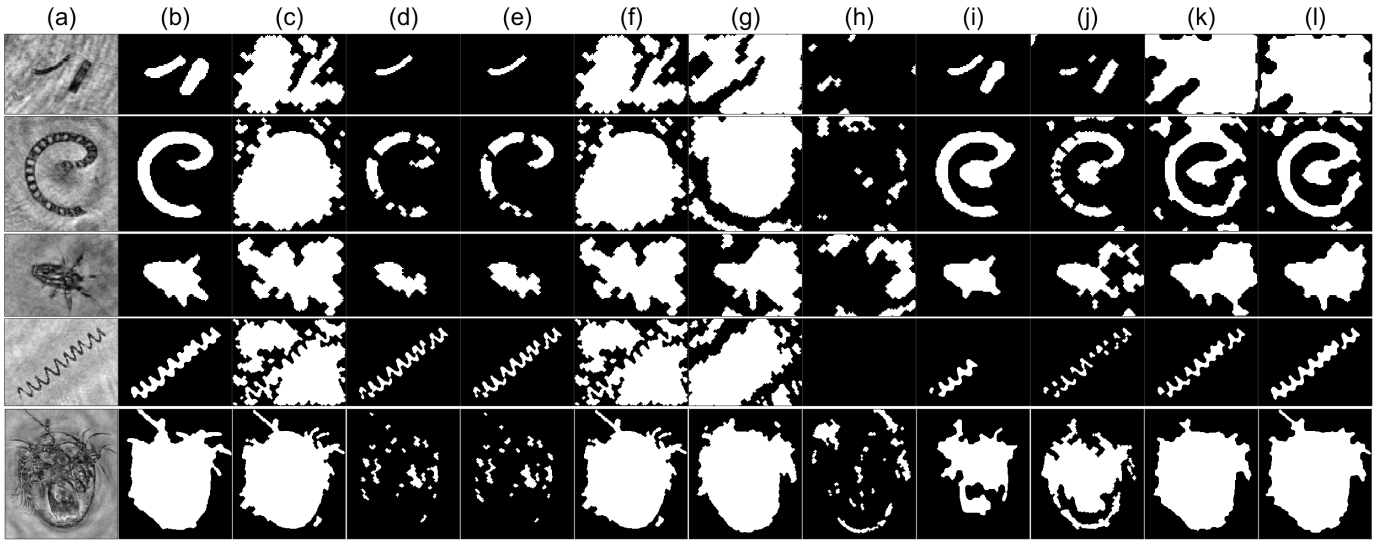

Fig. 4. Region extracted by the eleven methods from five example vignettes in the prediction dataset. (a) - original vignettes, (b) - structuredForest, (c) - cannyEdge, (d) - sobelEdge, (e) - prewittEdge, (f) - robertsEdge, (g) - activeContour, (h) - regionGrowing, (i) - SRegionMerging, (j) - watershed, (k) - OtsuThresholding, (l) - KMeans. Please note that the image size is adjusted for layout.

V. Size Estimation

The proposed method is lastly used to detect the particle regions from the (3257 + 1572) vignettes respectively extracted from the holograms in Events 034 and 098. The particle size information in these vignettes is calculated and estimated using the method described in Section Section III-C. The ESD of each particle region is calculated using Eq. (1). The particle size distribution versus depth is depicted in Fig. 5. These two profiles show similar trends of size distribution. Generally speaking, particle size reduces with increasing depth, and mean particle ESD obviously reduces from 50 m to 150 m (Event 034: ∼95 μm above 50 m and ∼62 μm below 150 m; Event 098: ∼91 μm above 50 m ∼66 μm below 150 m). Particle size throughout the water column was, on average, ∼87 μm in Event 034 and ∼88 μm in Event 098. Few particles whose ESDs are larger than 1,000 μm are detected at both observation sites. This could be due to either few particles at this size present in the sites when recording holograms or the failure of FastScan in reconstructing too large particles. Since we found some large particles larger/longer than 1,000 μm that were reconstructed by FastScan (three examples are shown in Fig. 6), we suggest that there were likely few particles larger than 1,000 μm appearing in the observation areas during hologram recording.

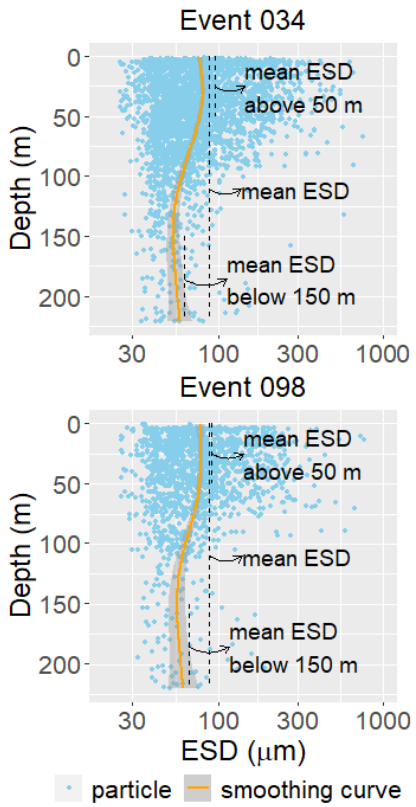

Fig. 5. Particle size distribution with depth in the two profiles estimated using the proposed method. The blue spots indicate the size of the particles, and the orange line is a smoothing curve of the spots in each diagram. The mean ESDs of the whole particles, the particles above 50 m and the particles below 150 m are respectively calculated.

VI. Conclusions and Discussion

Images provide much information on marine particle size which can aid to estimate vertical carbon fluxes in oceans. Due to high resolution and large-volume recording, LIDH is a powerful tool to image marine microscale particles. However, it is challenging to carry out rapid particle size extraction from holograms owing to time-expensive particle auto-focusing and much background noise in holograms. In this paper, a method

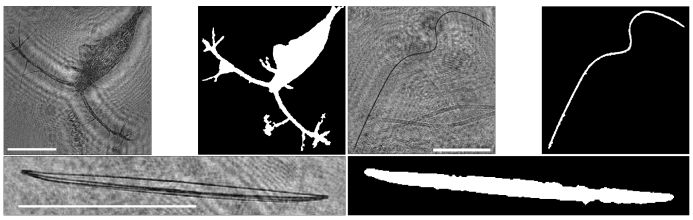

Fig. 6. Three large-size particles reconstructed by FastScan and their mask images extracted by the proposed method. Each white bar indicates 1,000 μm. Please note that the image size is adjusted for layout.

is developed to address this issue. There are four main findings based on the experiments in this work:
(1) The edge-detection model is respectively trained on 500 normal images and 500 synthetic holographic images, and the model trained on the holographic images significantly outperforms the model trained on the normal images (0.8257 $>$ 0.7028 in terms of SSIM).
(2) Amongst the eleven methods described in this work, the proposed method gives the highest accuracy ($\sim$0.7 of mean IoU) when extracting particle regions from 1,000 synthetic images; though it is not the fastest method, it can process 1,000 images within $\sim$25 seconds.
(3) The extracted regions by the proposed method from the given real holograms match real particle areas, even when there is more than one particle in the image.
(4) Synthetic data of marine particles is a useful alternative to human-annotated data for training a machine-learning-based model for object edge detection in holograms.

Therefore, we suggest that our method has the capability to rapidly extract particle regions from holographic images. This method was used to analyse the PSDs of two profiles recorded in South Georgia. The particle sizes were found to reduce with increasing depth. A sharp decline in the particle size is seen below 100 m. Few particles larger than 1,000 μm are detected at both observation sites.

However, some shortcomings exist in the proposed method:
(1) Fine features of particles are not well captured due to complicated background noise.
(2) Since the structured forest gives soft responses to particle edges in an input image, binarization is needed to generate a binary edge image.
(3) When generating a region mask for a particle, some morphological operations are needed to avoid breaking the detected particle region into several pieces (especially for transparent particles). However, these operations (such as hole filling) could result in the size of some particles being overestimated.

The first shortcoming could be improved via preparing a training dataset of synthetic holograms which are more like real holograms. The direct solution to the second shortcoming is to modify the model to output the determined edges for an input image, though this modification might affect the accuracy of edge detection. Regarding the last shortcoming, it is typically challenging to detect the regions of transparent particles in inline holograms due to weak scattering light from them and much background noise. This is a trade-off between detecting the entire area of a transparent particle into a single region and overestimating its size caused by morphological operations.

ACKNOWLEDGMENT

We thank Richard Lampitt, Morten Iversen and Kevin Saw for the deployment of the Red Camera Frame. Our thanks extend to the captain, crew and scientists of the research cruise DY086. This work was supported through the ANTICS project, receiving funding from the European Research Council (ERC) under the European Union's Horizon 2020 research and innovation programme (Grant Agreement No 950212). Data were collected as part of the COMICS project (Controls over Ocean Mesopelagic Interior Carbon Storage; NE/M020835/1) funded by the Natural Environment Research Council.

REFERENCES

[1] Serra-Pompei, C., Ward, B.A., Pinti, J., et. al., "Linking plankton size spectra and community composition to carbon export and its efficiency", Glob. Biogeochem. Cycles 36: e2021GB007275 (2022).
[2] mand, M.M., Govindarajan, R., He, J., et. al., "Sinking flux of particulate organic matter in the oceans: Sensitivity to particle characteristics", Sci. Rep. 10: 5582 (2020).
[3] Laurenceau-Cornec, E.C., Le Moigne, F.A.C., Gallinari, M., et. al., "New guidelines for the application of Stokes' models to the sinking velocity of marine aggregates", Limnol. Oceanogr. 65: 1264-1285 (2020).
[4] Lombard, F., Boss, E., Waite, A.M., et. al., "Globally consistent quantitative observations of planktonic ecosystems", Front. Mar. Sci. 6:196 (2019).
[5] Giering, S.L.C., Cavan, E.L., Basedow, S.L., et. al., "Sinking organic particles in the ocean—flux estimates from in situ optical devices", Front. Mar. Sci. 6:834 (2020).
[6] Giering, S.L.C., Culverhouse, P.F., Johns, D.G., et. al., "Are plankton nets a thing of the past? An assessment of in situ imaging of zooplankton for large-scale ecosystem assessment and policy decision-making", Front. Mar. Sci. 9:986206 (2022).
[7] Giering, S.L.C., Hosking, B., Briggs, N., et. al., "The interpretation of particle size, shape, and carbon flux of marine particle images is strongly affected by the choice of particle detection algorithm", Front. Mar. Sci. 7:564 (2020).
[8] Schnars, U., Falldorf, C., Watson, J., et. al., Digital Holography and Wavefront Sensing, Springer, Berlin, Heidelberg, 2015.
[9] Aditya, N., Ed, M., Malcolm, M., et. al., "A review of holography in the aquatic sciences: in situ characterization of particles, plankton, and small scale biophysical interactions", Front. Mar. Sci. 7: 572147 (2021).
[10] Yang, Y., and Kang, B., "Determination of depth-of-focus in lensless in-line digital particle holography", Optik 122(17): 1552-1557 (2011).
[11] Graham, G.W. and Nimmo-Smith, W.A.M., "The application of holography to the analysis of size and settling velocity of suspended cohesive sediments", Limnol. Oceanogr. Methods 8: 1-15 (2010).
[12] Yu, S., Chen, M., Zhang, E., et. al. "Robustness study of noisy annotation in deep learning based medical image segmentation", Phys. Med. Biol. 65(17): 175007 (2020).
[13] Mahdaviara, M., Shojaei, M.J., Siavashi, J., et. al., "Deep learning for multiphase segmentation of X-ray images of gas diffusion layers", Fuel 345: 128180 (2023).
[14] Hassen Mohammed, H., Elharrouss, O., Ottakath, N., et. al., "Ultrasound intima-media complex (IMC) segmentation using deep learning models", Appl. Sci 13: 4821 (2023).
[15] Burns, N. and Watson, J., "Robust particle outline extraction and its application to digital in-line holograms of marine organisms", Opt. Eng. 53(11): 112212 (2014).
[16] Dollár, P. and Zitnick, C.L., "Fast Edge Detection Using Structured Forests," IEEE Trans. Pattern Anal. Mach. Intell. 37(8): 1558-1570 (2015).

[17] LISST-HOLO User's Guide, Ch. 2: 11-13, https://www.comm-tec.com/Docs/Manuali/Sequoia/LISST-HOLO-manual-v3.0.pdf, visited on Apr. 10, 2023.
[18] Sanders R.J., Henson S.A., Martin A.P., et. al., "Controls over ocean mesopelagic interior carbon storage (COMICS): fieldwork, synthesis, and modeling efforts. Front. Mar. Sci. 3: 136 (2016).
[19] Liu, Z., Giering, S., Takahashi, T., et. al. "Advanced subsea imaging technique of digital holography: in situ measurement of marine microscale plankton and particles", 2023 IEEE Underwater Technology Symposium, Tokyo, Japan, March 06-09, 2023.
[20] Thevar, T., Burns, N., Ockwell, M., et. al., "An Ultracompact Underwater Pulsed Digital Holographic Camera With Rapid Particle Image Extraction Suite," IEEE J. Ocean. Eng., Early Access: doi: 10.1109/JOE.2022.3220880.
[21] Giering, S. L.C., Wells, S.R., Mayers, K.M.J., "Seasonal variation of zooplankton community structure and trophic position in the Celtic Sea: A stable isotope and biovolume spectrum approach", Prog. Oceanogr. 177: 101943 (2019).
[22] Otsu, N., "A threshold selection method from gray-level histograms", IEEE Trans. Sys. Man. Cyber. 9(1): 62-66 (1979).
[23] The BSDS500, The Berkeley Segmentation Dataset and Benchmark, https://www2.eecs.berkeley.edu/Research/Projects/CS/vision/bsds/, visited on Apr. 10, 2023.
[24] Wang, Z., Bovik, A., Sheikh, H., et. al., "Image quality assessment: from error visibility to structural similairty", IEEE Trans. Image Process. 13(4): 600-612 (2004).
[25] Find edges in 2D grayscale images using MATLAB, https://uk.mathworks.com/help/images/ref/edge.html, visited on Apr. 10, 2023.
[26] Segment image into foreground and background using active contours (snakes) region growing technique using MATLAB, https://uk.mathworks.com/help/images/ref/activecontour.html, visited on Apr. 10, 2023.
[27] Kroon, D., "Region Growing", MATLAB Central File Exchange, https://www.mathworks.com/matlabcentral/fileexchange/19084-region-growing , visited on Apr. 10, 2023.
[28] Boltz, S., "Image segmentation using statistical region merging", MATLAB Central File Exchange, https://www.mathworks.com/matlabcentral/fileexchange/25619-image-segmentation-using-statistical-region-merging, visited on Apr. 10, 2023.
[29] Eddins, S., "Watershed transform question from tech support", MATLAB Central Blogs, https://blogs.mathworks.com/steve/2013/11/19/watershed-transform-question-from-tech-support/?s_tid=srchtitle_Watershed%20Transform_1, visited on Apr. 10, 2023.
[30] Global image threshold using Otsu's method using MATLAB, https://uk.mathworks.com/help/images/ref/graythresh.html, visited on Apr. 10, 2023.
[31] K-means clustering based image segmentation using MATLAB, https://uk.mathworks.com/help/images/ref/imsegkmeans.html, visited on Apr. 10, 2023.